TOPOLOGICAL DERIVATIVE-BASED FRACTURE MODELLING IN BRITTLE MATERIALS: A PHENOMENOLOGICAL APPROACH

M. XAVIER, E.A. FANCELLO, J.M.C. FARIAS, N. VAN GOETHEM, AND A.A. NOVOTNY

Abstract. The Griffith-Francfort-Marigo damage model describes the behavior of brittle materials under the quasi-static loading assumption, focusing on the evolution of damage regions. It is based on the minimization of a shape functional given by the sum of the total potential energy of the system with a Griffith-type dissipated energy, with respect to the distribution of the healthy and damaged phases, under an irreversibility constraint. A natural approach to deal with such a minimization problem consists in considering the topological derivative concept to nucleate small damaged regions and the shape gradient to propagate them. In contrast to such an approach, in this paper the Griffith-Francfort-Marigo damage model is revisited by using the sole tool of topological derivative. In particular, we propose a striking simple numerical scheme based on the computation of the topological derivative field to determine damage nucleation as well as crack/damage propagation. In other words, the topological derivative is used as descent direction to minimize the Francfort-Marigo functional indicating, in each iteration, the regions that have to be damaged. Therefore, the proposed topology optimization algorithm is able to capture the whole nucleation and propagation damaging process, including important features like kinking and bifurcations. These properties are confirmed through several numerical experiments and by comparison with available laboratory experiments.

1. Introduction

Many works in Fracture Mechanics address the issue of microscopic modelling of fractures and the coupling of some defect atomistic models with macroscopic elasto-plastic models. In this paper, we focus on a purely macroscopic model in the framework of continuum mechanics. Roughly speaking, continuum models can be classified in two main categories. On the one hand, there are models of crack growth and propagation which assume that the crack is a surface evolving in three-dimensional body, with specific evolution laws, which are found innumerable in Fracture literature (often depending on the body shape and dimensions). On the other hand, one can consider models of fracture, where the crack is identified with a thin damage. In this case there exists a competition between the initial healthy elastic phase and another damaged elastic phase. The transition from healthy to damaged can be smooth or sharp, i.e., there is an interface between a healthy and a fully damaged zone. Our model belongs to this second class.

The origin of such a model amounts to the British engineer A.A. Griffith in 1921, who published a paper on fracture of glass. In this work, Griffith assumes that flaws pre-exist in the body, where stress concentrates, provoking atomic debonding and resulting in crack propagation, until the body breaks. The pre-existing crack is submitted to an external load: force or imposed displacement. In Griffith's model, the system is modeled by two thermodynamic variables: the area of the crack and the displacement of the loading grips. The energy of the system is the sum of the elastic energy in the body, and the surface energy of the crack, and is a function of a single thermodynamic variable: the area of the

Key words and phrases. Topological derivative, Francfort-Marigo damage model, Topology optimization algorithm.

crack. When the crack evolves, the stress in the sample is partially relieved, so that the elastic energy is reduced. At the same time, the advancing crack creates more surface area, so that the surface energy increases. Thermodynamics dictates that the process should go in the direction that reduces the total available free energy. If the decrease in elastic energy prevails, the crack grows, otherwise the crack heals. Specifically, let U be the internal energy (i.e., the macroscopic energy of the atoms), P be the work of the volume and surface forces (i.e., $-P$ is the potential energy), S be the body entropy and T_0 the surface temperature, assumed constant and equal to the ambient temperature. Let us assume that the process is quasi-static, the kinetic energy and the volume heat sources are negligible, whereas the surface heat supply must not vanish a-priori (recall that boundary loads are prescribed). Therefore the combination of the first and second laws of Thermodynamics yields

$$\frac{d}{dt}(U - P - T_0 S) \leq 0, \tag{1.1}$$

where Griffith takes U as the sum of the stored elastic energy E and a surface term proportional to the crack area, D. Thus, Griffith's Law (1.1) strictly tells us that the available free energy must decrease in time, that is that the total energy $\mathcal{F} := E - P + D$ tends to be minimized, while the entropy S increases.

A stronger postulate was considered about 70 years later by Francfort and Marigo [12] when revisiting Griffith's model under the framework of global minimization of the energy. Indeed, the authors, and after them a series of coworkers and contributors did suppose that at each quasi-static step, the total energy $\mathcal{F}$ assumes a global minimum with respect to the distribution of the healthy and damaged phases. Furthermore, they assumed that the crack is irreversible, meaning that healing is precluded: at each step, either the crack is unchanged, and hence load is increased, either the crack advances, and hence its area is strictly increasing.

There are several ways to compute the minimum of the energy in order to provide a computational algorithm of fracture/damage propagation (see, e.g., [11]). One minimization scheme suggested in [1] relies on shape optimization principles. It consists of a descent method driven by the shape gradient of the energy functional, i.e., the energy decreases in the normal direction to the boundary of the damage region with a magnitude given by the shape derivative of $\mathcal{F}$. Furthermore, in order to nucleate new damage regions, the so-called topological derivative of $\mathcal{F}$ was also considered in [1]. Let us emphasize that in theory the concepts of shape and topological derivatives are distinct, and the latter is computed in the undamaged part of the body, in order to determine if it is energetically worth to create some new damage away from the existing one. One drawback of using the shape gradient approach, is in fact that it is a vector field concentrated on the boundary of the damage, as opposed to the topological derivative which is a scalar field distributed in the whole domain. Therefore, one needs a very good computation of the normal vector to the damage region, because this vector will determine the crack/damage path. It turns out that the shape optimization method of [1] was promising, but computationally expensive.

Topological sensitivity analysis may be considered for a pure fracture model as in [19, 16] as for a damage model with crack-like damage regions. It is the purpose of the present work to revisit Griffith-Francfort-Marigo damage model by using solely the topological derivative concept, that is, the computation of this scalar quantity should allow us to determine damage nucleation as well as crack/damage propagation, relying on the contour lines of the topological derivative field. It can be proven, but is not the aim of this

work, that from a theoretical standpoint the concepts of shape and topological derivatives do coincide on the boundary of the damage region [6]. In this work, we present a simple numerical scheme that was able to improve the results of [1], not only in terms of computational cost but also in terms of successful crack propagation assessment tests. The interest of this method is its striking simplicity: to achieve minimization, a single scalar field is computed from which nucleation and propagation of damages are determined. In particular, the topological derivative is used as descent direction to minimize the Francfort-Marigo functional indicating, in each iteration, the regions that have to be damaged. Therefore, the proposed topology optimization algorithm is able to capture the whole nucleation and propagation damaging process, including important features like kinking and bifurcations. These properties are confirmed through several numerical experiments, whose results are compared with real laboaratory tests when available. Let us emphasize however that being a descent method, what is actually achieved is local rather than global minimization, which is also more sound from a Physical perspective. In this respect, our choice has been to refine the mesh at the crack tip as soon as a local advance is made. In such a way, according to our numerical results, bifurcation and kinking are rather well captured.

The paper organized as follows. The Griffith-Francfort-Marigo damage model is revisited in Section 2. Its associated topological derivative is presented in Section 3. The resulting topology optimization algorithm is shown in all its details through Section 4. The obtained numerical results are presented in Section 5, where the whole nucleation and propagation damaging process is observed, together with important features such as kinking and bifurcations. Finally, the paper ends with some concluding remarks in Section 6.

2. Mechanical Model

The Griffith-Francfort-Marigo damage model describes the behavior of brittle materials under the quasi-static loading assumption, focusing on the evolution of damage regions [12]. Unlike ductile materials, perfectly brittle materials show no irreversible deformation and no energy dissipation immediately before the crack propagation, and thus the failure is usually brutal. Based on this evidence, the damage model of Francfort-Marigo asserts that an abrupt change in the material behavior takes place pointwisely.

The main idea behind this type of damage model is to introduce an elastic body made of two distinct materials, here represented by the parameter $\rho_0 \ll 1$. The change from the original material to the damaged one occurs only if the elastic energy released by this transition overcomes a certain material-dependent threshold. In other words, the occurrence of the damage is determined by the relation

$$\frac{1}{2}\mathbb{C}\varepsilon \cdot \varepsilon - \frac{1}{2}\rho_0 \mathbb{C}\varepsilon \cdot \varepsilon > \kappa \,, \tag{2.1}$$

where $\mathbb{C}$ is the fourth-order elasticity tensor, ε is the second order strain tensor and κ is a material property that represents the damage toughness.

Two conditions are expected for this model. Firstly, the health material should be more stiffer than the damaged material, i.e.,

$$(1-\rho_0)\mathbb{C}\varepsilon \cdot \varepsilon > 0 \quad \forall \varepsilon \,, \tag{2.2}$$

to characterize the stiffness loss associated with the damage. Secondly, the damage ($\mathbb{C} \to \rho_0\mathbb{C}$) is permanent, i.e., the material is unable to return to its original state ($\rho_0\mathbb{C} \not\to \mathbb{C}$). Thus, irreversibility imposes a constraint on the evolution of the phenomenon.

More precisely, let us consider an open and bounded geometrical domain $\Omega \subset \mathbb{R}^2$, with Lipschitz boundary $\Gamma := \partial\Omega$, and a sub-domain ω of the form $\omega \subset \Omega$. Francfort and Marigo proposed a functional that should be minimized at each time instant t_i, whose arguments are the displacement field u_i and the damage distribution $\rho : \Omega \to \{1, \rho_0\}$ defined as

$$\rho(x) := \begin{cases} 1, & \text{if } x \in \Omega \setminus \overline{\omega}, \\ \rho_0, & \text{if } x \in \omega. \end{cases} \tag{2.3}$$

Since $\rho_0 \ll 1$, $\Omega \setminus \overline{\omega}$ and ω are used to represent the health and damage parts of the elastic body, respectively. That is, if $\rho(x) = 1$ one recovers the health material $\mathbb{C}$, otherwise, if $\rho(x) = \rho_0$ one obtains the damaged material $\rho_0\mathbb{C}$.

The Francfort-Marigo functional $\mathcal{F}_\omega(u_i)$ is defined as the sum of the total potential energy and an energy dissipation term, namely

$$\mathcal{F}_\omega(u_i) = \mathcal{J}(u_i) + \kappa|\omega|, \tag{2.4}$$

where $|\omega|$ is the Lebesgue measure of ω and $\mathcal{J}(u_i)$ is the total potential energy defined as

$$\mathcal{J}(u_i) = \frac{1}{2}\int_\Omega \sigma(u_i) \cdot \varepsilon(u_i)\, d\Omega \,. \tag{2.5}$$

Note that there are no body forces, nor surface tractions. Indeed, we are going to impose a nonhomogeneous Dirichlet boundary condition, i.e., a prescribed displacement. Some term in the above equation require explanation. The stress tensor $\sigma(\varphi)$ is defined as

$$\sigma(\varphi) = \rho\mathbb{C}\varepsilon(\varphi) \,, \tag{2.6}$$

while the strain tensor $\varepsilon(\varphi)$ is given by the symmetric part of the gradient of φ, namely

$$\varepsilon(\varphi) = \frac{1}{2}(\nabla\varphi + (\nabla\varphi)^\top) \,. \tag{2.7}$$

We restrict ourselves to isotropic material, so that the elasticity tensor $\mathbb{C}$ can be represented by the Lamé's coefficients μ and λ in the following form

$$\mathbb{C} = 2\mu\mathbb{I} + \lambda(\mathrm{I} \otimes \mathrm{I}) \,, \tag{2.8}$$

where I and $\mathbb{I}$ are the second and fourth identity tensors, respectively. Finally, the displacement field is solution to the following boundary value problem: Find u_i, such that

$$\begin{cases} \mathrm{div}\sigma(u_i) &=& 0 & \text{in } \Omega, \\ \sigma(u_i) &=& \rho\mathbb{C}\varepsilon(u_i), & \\ u_i &=& g_i & \text{on } \Gamma_D, \\ \sigma(u_i)n &=& 0 & \text{on } \Gamma_0. \end{cases} \tag{2.9}$$

where $g_i = g_{i-1} + \Delta g_i$ is used to denote a prescribed displacement on the boundary $\Gamma_D \subset \Gamma$ depending on the time instant t_i and the increment Δg_i. Thus, the total applied displacement g is computed as the sum

$$g = g_0 + \sum_{i=1}^{N} \Delta g_i \,, \tag{2.10}$$

where N is the total number of increments. Finally, $\Gamma_0 \subset \Gamma$ is used to denote a traction free boundary. Therefore, $\Gamma = \Gamma_D \cup \Gamma_0$, such that $\Gamma_D \cap \Gamma_0 = \emptyset$.

Now, we have all elements to state the Francfort-Marigo damage model, which consists in minimizing the functional $\mathcal{F}_\omega(u_i)$, for each time increment t_i, with respect to the set $\omega \subset \Omega$. That is

$$\underset{\omega\subset\Omega}{\text{Minimize}}\ \mathcal{F}_\omega(u_i), \text{ subject to (2.9)} \,. \tag{2.11}$$

This model is purely energetic in the sense that damage evolution is based just on the energy density distribution. As a direct consequence, it is not able to distinguish the difference between traction and compression stress states and thus not suited to describe the crack closure phenomenon.

Another important feature of the model concerns the characterization of a critical load. In problems without singularities, critical load is the one that allows local strain-energy density to achieve a critical value. In problems with stress singularities, however, the strain energy density rises locally to unbounded values and consequently above any finite threshold. Nevertheless, experiments like those of Griffith indicate the existence of a critical nonzero load even in the presence of such singularities, which reveals a limitation on the straightforward application of the Francfort-Marigo model in these cases. An existing remedy in the literature proposes a modification in the (discrete) numerical scheme of the model by introducing a new material property κ_s used in conjunction with a scaling factor associated with a mesh size measure [1]. Here, we replace κ by a modified energy release parameter κ_δ (see (2.1)) defined by the ratio

$$\kappa = \kappa_\delta := \frac{\kappa_s}{\delta} \,, \tag{2.12}$$

where δ is a scaling factor associated with the width of the initial damage. From the physical point of view, when δ becomes smaller, the parameter κ_δ increases in a similar way as the energy density, so that the critical load converges to a finite nonzero value. This strategy has shown to be effective in problems of crack propagation where the fracture is represented by a damaged region of small width δ, since letting $\delta \to 0$ forces the damage region to be crack-like. In the original Bourdin, Francfort and Marigo work [11], the crack was approximated by a smeared region by Ambrosio and Tortorelli functional [2], whereas in our approach the contrary is done: a damage converges to a crack. In the anti-plane case theoretical results in this respect were derived by Dal Maso and Iurlano [17]. Note the use of κ_s is explicitly taken into account in these approximations. See also [15], where a phenomenological continuum model for mode III dynamic fracture based on the phase-field approach is proposed.

3. Topological Derivative

In order to solve the minimization problem (2.11), we use the topological derivative concept [18]. The idea is to evaluate the topological derivative of the shape functional (2.4) with respect to the nucleation of a small circular inclusion. Such a topological derivative is know in the literature. For the sake of completeness, we state the main result to be used in this paper, which is given by the following theorem [18, Ch. 5, pp. 158]:

Theorem 1. *The topological derivative of the shape functional* (2.4) *with respect to the nucleation of a small circular inclusion with different material property from the background, represented by a contrast γ, is given by the sum*

$$D_T\mathcal{F}_\omega(x) = D_T\mathcal{J}(x) + \kappa_\delta D_T|\omega|(x) \quad \forall x \in \Omega \,. \tag{3.1}$$

The last term $D_T|\omega|(x)$ is trivially given by

$$D_T|\omega|(x) = \begin{cases} +1, & \text{if } x \in \Omega \setminus \overline{\omega}, \\ -1, & \text{if } x \in \omega, \end{cases} \tag{3.2}$$

while the first term $D_T\mathcal{J}(x)$ is known, whose closed formula is written as

$$D_T\mathcal{J}(x) = -\mathbb{P}_\gamma \sigma(u_i(x)) \cdot \varepsilon(u_i(x)) \,, \tag{3.3}$$

where the polarization tensor $\mathbb{P}_\gamma$ *is given by the following fourth order isotropic tensor*

$$\mathbb{P}_\gamma = \frac{1}{2}\frac{1-\gamma}{1+\gamma a_2}\left((1+a_2)\mathbb{I} + \frac{1}{2}(a_1-a_2)\frac{1-\gamma}{1+\gamma a_1}\mathrm{I}\otimes\mathrm{I}\right), \tag{3.4}$$

with the parameters a_1 *and* a_2 *given by*

$$a_1 = \frac{\lambda+\mu}{\mu} \quad \textit{and} \quad a_2 = \frac{\lambda+3\mu}{\lambda+\mu}, \tag{3.5}$$

and the contrast γ *is defined as follows*

$$\gamma(x) = \begin{cases} \rho_0, & \textit{if } x \in \Omega \setminus \overline{\omega}, \\ \rho_0^{-1}, & \textit{if } x \in \omega. \end{cases} \tag{3.6}$$

See also [3, 5] *for details on the formula derivations. The same formula* (3.3) *holds true for heterogeneous medium* [13]*, provided that the heterogeneity is locally Lipschitz continuous.*

Let us remark that we have here chosen the same contrast for each of the two Lamé's coefficients. For the expression of the topological derivative with a distinct contrast, we refer to [1]. In this reference it is also proven that $D_T\mathcal{J}(x) < 0$ if $x \in \Omega \setminus \overline{\omega}$ and $D_T\mathcal{J}(x) > 0$ if $x \in \omega$ (see [1, Theorem 4.1]).

4. Resulting Algorithm

The topological sensitivity analysis provides a first order correction for the shape functional when an infinitesimal perturbation is introduced in the domain. Therefore, it is possible to decrease the value of the shape functional by introducing infinitesimal inclusions at the regions where the topological derivative is negative. Since due to practical reasons only finite size perturbations can be created, we propose an algorithm based on the introduction of an inclusion of finite size at the region where the topological derivative is negative. If the size of the inclusion is small enough, but at the same time large enough to be treated numerically, it is expected that the Francfort-Marigo functional decreases. The size of inclusion is associated with the region ω^* where the topological derivative field is negative, i.e.,

$$\omega^* := \{x \in \Omega : D_T\mathcal{F}_\omega(x) < 0\} \ . \tag{4.1}$$

In principle ω^* must not be a connected subset, that is, there might be nucleation of damage in front of the previously damage zone, but also elsewhere in the body. In the former case, nucleation of damage yields evolution of the damage set, whereas in the latter it means genuine damage nucleation. Let us emphasize that from a theoretical point of view, the topological derivative holds away from the damage region and for an infinitesimal inclusion only. On the other hand, the topological derivative can be used as a steepest-descent direction in the optimization process like in any method based on the gradient of the objective functional. Therefore, for practical purposes, since the numerical method introduces a grid of finite size, we will consider nucleation of inclusions of finite sizes but small enough such that a decreasing of the Francfort-Marigo functional in each iteration is ensured. It should also be noted that it can be proved that the topological gradient can be used in place of the shape gradient (as done in [1]) to compute the time evolution of the damage region.

Having said that, at this stage, we are free to design our algorithm either by nucleating only at those points where the topological derivative achieves its minimum, or at all points were it is negative, while an intermediate choice would be to calibrate the size of the inclusion to be nucleated according to the characteristic size of the previously damaged region. This choice will be provided by the model parameter $\beta \in (0, 1)$, with the extreme

choices given by $\beta = 0$ (minimum points only), and $\beta = 1$ (the whole negative region), respectively. To this aim, let us introduce the quantity

$$D_T\mathcal{F}_\omega^* := \min_{x\in\omega^*} D_T\mathcal{F}_\omega(x) \ , \tag{4.2}$$

which allows us to define the inclusion to be nucleated $\omega^\beta \subset \omega^*$ as follows

$$\omega^\beta := \{x \in \omega^* : D_T\mathcal{F}_\omega(x) \leq (1-\beta)D_T\mathcal{F}_\omega^*\} \ , \tag{4.3}$$

where $\beta \in (0,1)$ is chosen such that $|\omega^\beta| \approx \pi\delta^2/4$ (and $|\omega^\beta| \leq \pi\delta^2/4$), so that the size of the inclusion to be nucleated is here related to the width of the initial damage δ. Therefore, if the initial damage is crack-like (δ small), β will be taken as small as to satisfy $|\omega^\beta| \leq \pi\delta^2/4$. By this choice, a damage will evolve like a crack. As a matter of fact, the parameter β induces a threshold for the topological derivative $D_T\mathcal{F}_\omega(x)$ and the volume of the inclusion will only depend on δ, while its shape will depend on the contour lines (level-sets) of $D_T\mathcal{F}_\omega$. We will show through some numerical experiments that this strategy ensures a decreasing of the Francfort-Marigo functional in each iteration, provided that the size of the inclusion to be nucleated ω^β is small enough.

The algorithm can be outlined as follows. Given the solution of the linear elasticity system (2.9), the associated topological derivative field (3.1) is evaluated. If the field is positive everywhere or $|\omega^*| < \pi\delta^2/4$, a perturbation of size $\pi\delta^2/4$ at any point of the domain is likely to increase the value of the functional. In this case, the algorithm will not propagate the damage, and it is possible to increase the load g_i further and run a new analysis. On the contrary, if the topological derivative field is negative in some undamaged region and the condition $|\omega^*| \geq \pi\delta^2/4$ is fulfilled, a damage ω^β will be nucleated inside ω^*, with $\beta : |\omega^\beta| \approx \pi\delta^2/4$ (and $|\omega^\beta| \leq \pi\delta^2/4$). Schematically, one can see the newly-damaged region as an half-disk of radius $\delta/2$ located at the tip of the pre-existing damage. Since the nucleation of a new damage ω^β modifies the problem, the solution to the elasticity system associated with the new topology have to be computed again. Finally, the new topological derivative field is evaluated and the process is repeated until the condition $|\omega^*| \geq \pi\delta^2/4$ is not fulfilled anymore for any load increment. The elasticity system is solved by the Finite Element Method. In order to improve the numerical results, the mesh at the crack tip is intensified in each iteration of the optimization process. The above procedure written in the form of pseudo-code is given in Algorithm 1.

5. Numerical Experiments

The elasticity problem is discretized by using linear triangular elements only. It should be emphasized that the boundary conditions induces a stress concentration and it is therefore natural to expect damage initiation at these locations. However, in order to compare our results with those found in the literature, the regions near to the boundary conditions were ignored. The damage evolution are represented by black and red lines. The black trajectories represent the damage evolution in a material traction state, $\mathrm{tr}(\sigma(u_i(x))) > 0$, whereas the red trajectories represent the damage evolution in a compressive (unphysical) state $\mathrm{tr}(\sigma(u_i(x))) < 0$.

5.1. **Mode I Opening.** The first example considers the Mode I crack opening. This case will be used as a reference to calibrate the necessary parameters and check the overall performance of Algorithm 1. The domain consists of a unit square $\Omega = (0,1)\times(0,1)$ with unit thickness (units are in m) with an initial damage of length h and width δ located in the center of the left side of the domain, as shown in Figure 1. A vertical displacement was imposed on the bottom and top sides of the domain with a total intensity g, which has been divided into 100 uniform load increments. The material properties modulus of

Algorithm 1: The damage evolution algorithm.

input : Ω, ω, δ, N, g_0, Δg_i
output: The optimal topology $\omega^\star$

for $i = 1 : N$ **do**
  solve elasticity system (2.9);
  evaluate the topological derivative $D_T\mathcal{F}_\omega$ according to (3.1);
  compute the threshold ω^* from (4.1);
  while $|\omega^*| \geq \pi\delta^2/4$ **do**
    intensify the mesh at the crack tip;
    solve elasticity system and evaluate $D_T\mathcal{F}_\omega$;
    compute the threshold ω^* from (4.1);
    compute the threshold ω^β from (4.3);
    nucleated new inclusion ω^β inside ω^*;
    update the damaged region: $\omega \leftarrow \omega \cup \omega^\beta$;
    solve elasticity system and evaluate $D_T\mathcal{F}_\omega$;
    compute the threshold ω^* from (4.1);
  end while
end for

elasticity E, Poisson ratio ν, and energy release rate κ_s correspond to the high-strength concrete. The inclusion is made of a material with an elasticity modulus $\rho_0 E$ and its diameter is specified by the parameter l. All these data are summarized in Table 1.

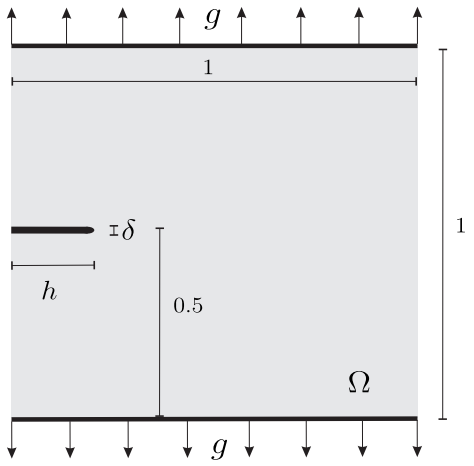

FIGURE 1. Mode I. Geometry and boundary conditions.

TABLE 1. Mode I. Parameters.

Parameter	Value	Parameter	Value
h	0,25 m	E	30 GPa
δ	0,01 m	ρ_0	10^{-6}
l	$2\delta/3$ m	ν	0,20
g	0,01 m	κ_s	3.2×10^6 J/m

5.1.1. *Critical Load.* The Francfort-Marigo damage model is not suited for the determination of a critical load in problems with singularities, such as the limiting case when $\delta \to 0$ of the Mode I example. In this case any non-null load is sufficient to raise infinitely the value of the energy density at the crack tip. When it is of interest to characterize a critical load in problems that have initial damage, a strategy can be chosen in a similar manner as in [1]. As discussed in Section 2 instead of using the mesh size, we chose to use as a scale factor a dimension associated with the geometry of the problem, given by the initial width δ of the damaged region. Hence, as the width δ of the initial damage is reduced, the parameter κ_δ grows in order to compete against the increase of the elastic energy density at the damage tip. To verify this assertion, five tests were made with different values for the initial width, namely $\delta \in \{\frac{1}{20}, \frac{1}{40}, \frac{1}{80}, \frac{1}{160}, \frac{1}{320}\}$[m]. The parameters were maintained according to Table 1.

The critical load g_c was selected as the value of the displacement boundary condition which allows the nucleation of the first inclusion, that is, when the condition $|\omega^*| \geq \pi\delta^2/4$ holds for the first time. Figure 2 illustrates the critical load obtained for the different experiments, which are normalized according to the first estimate found for the critical load g_c^0. Therefore, the introduction of the *ad hoc* parameter κ_δ through (2.12) allows for dealing with a feasible critical loading for $\delta > 0$, as shown in Figure 2 (dashed-bullet line). We claim however that the limiting case $\delta \to 0$ is much more involved and has been considered in [19], for instance.

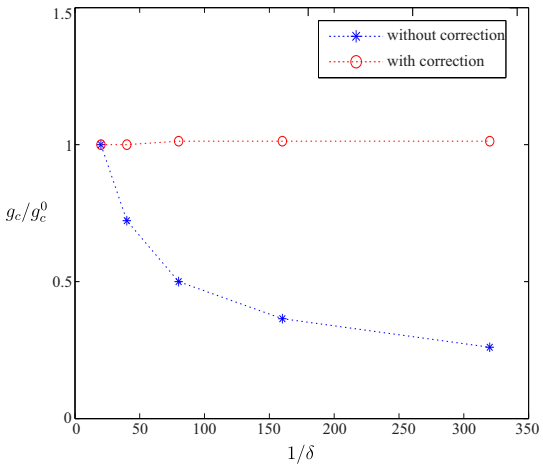

FIGURE 2. Mode I. Convergence analysis for the critical load.

As expected, with the decrease of the width δ, the energy density at the damage endpoint increases. Note that without a scale factor correction, the critical load decreases towards zero. On the other hand, the use of the factor δ leads to an asymptotic behavior for the critical load. Therefore, to describe completely the model, it remains to calibrate the parameter κ_s according to experimental data.

5.1.2. *Damage Evolution.* After this preliminary analysis, the experiment was simulated using the parameters shown in Table 1. The topological derivative at the crack tip at the precise time before the propagation can be seen in details in Figure 3(a). The distribution of damage at the end of the optimization process can be seen in Figure 3(b).

The result is similar to those obtained in [1], and as expected the damage growth took place in traction (see the damage in black). The history of the strain energy can be seen in Figure 4(a). It is observed that the damage region remains unchanged until the increment $i = 80$. Therefore, damage propagation took place between the load increments

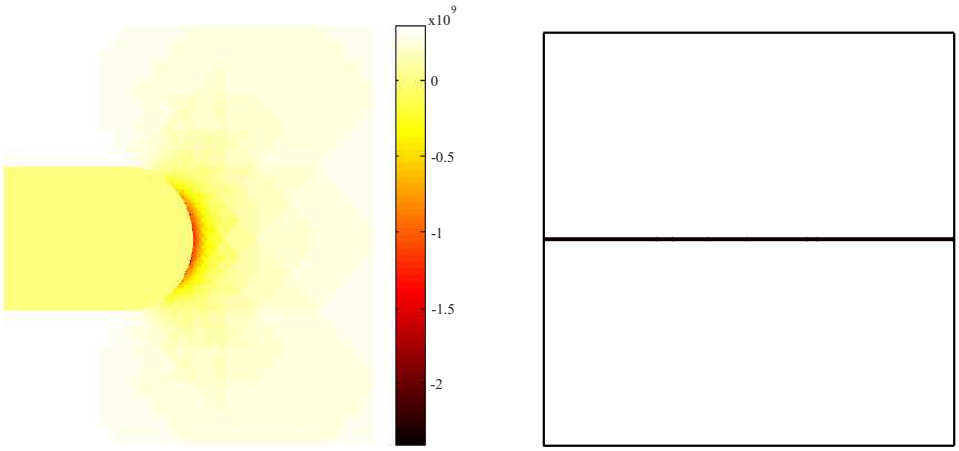

(a) topological derivative (b) final damage path

FIGURE 3. Mode I. Damage evolution.

80 and 81. Note the abrupt drop in the strain energy between these two load increments. In the following load increments $(81 - 100)$, the material also acquires a strain energy due to the residual material stiffness, though not noticeable due to its low value. The topology optimization processes starts in the load increment 80, whose history of the shape functional can be seen in Figure 4(b). Note that the model dissipates energy in all iterations.

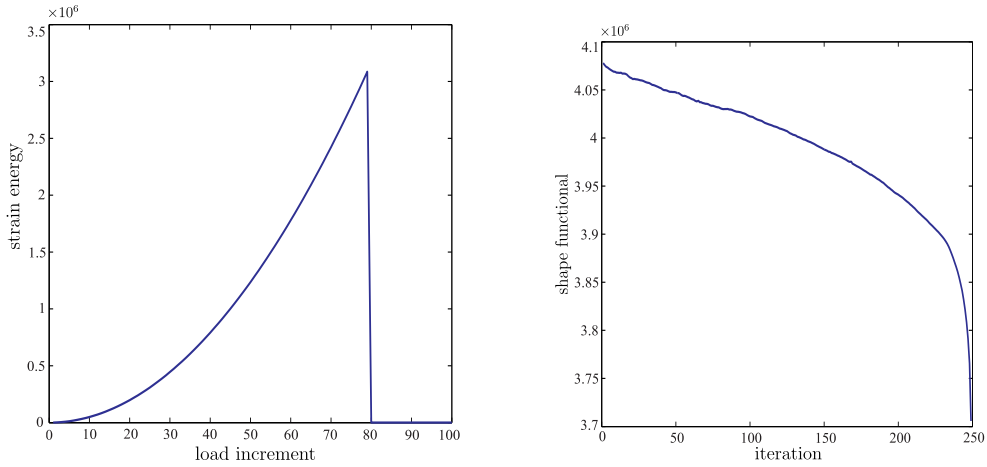

(a) strain energy $\mathcal{J}(u_i)$ from (2.5) (b) total energy $\mathcal{F}_\omega(u_i)$ from (2.4)

FIGURE 4. Mode I. Obtained histories.

The initial mesh has 47746 elements and 24076 nodes, while the final mesh has 121160 elements and 60797 nodes. The total CPU time of the whole process was 1h and 7min in a PC endowed with 3.4GHz processor and 16GB of RAM memory.

5.2. **Nucleation Phenomenon.** This example has the same geometry end boundary conditions of the Mode I case. The parameters are the same observed in Table 1 except by κ_s, which is set as $\kappa_s = 1.0 \times 10^6 J/m$. However, a hole of radius $r = 0.1m$ located in the center of the square is introduced, as shown in Figure 5. The obtained result can be seen in Figure 6(a). It can be verified that the proposed algorithm was able to activate the mechanism of damage nucleation, independently of any initial damaged region on

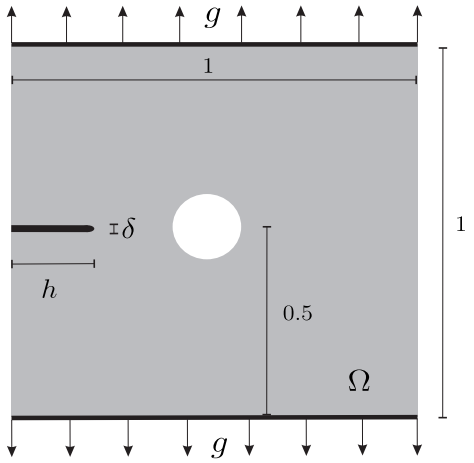

FIGURE 5. Nucleation phenomenon. Geometry and boundary conditions.

the boundary of the hole. Note that the strain energy increases before the nucleation phenomenon, Figure 6(b).

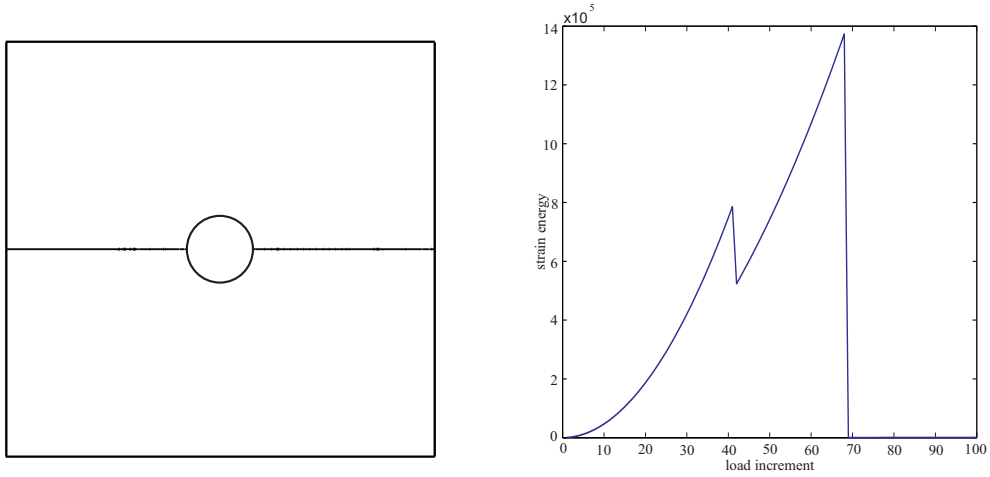

(a) final damage path (b) strain energy $\mathcal{J}(u_i)$ from (2.5)

FIGURE 6. Nucleation phenomenon.

5.3. **Mode II Opening.** The next case aims at revealing the capability of Algorithm 1 to create branches of damaged regions. The mode II test case has a similar geometry as that of mode I, differing only in the type of boundary condition. In this case, there are opposite and tangent displacement conditions at the top and bottom faces, as shown in Figure 7. In a similar manner to the first case, the parameters used are given in Table 2.

As discussed, the Francfort-Marigo model is energetic and for this reason it does not distinguish between states of traction and compression. It is nevertheless possible to adopt a heuristic numerical scheme to test different damage evolutions according to this procedure. To this aim, a test which checks if the trace of the stress tensor is positive, namely $\mathrm{tr}(\sigma(u_i(x))) > 0$, can be made. If negative, the damage will not be created even if the topological derivative is negative. Unlike [4], where the functional is modified to incorporate the distinction between traction and compression, our approach is purely algorithmic and investigative. However for clarity, the two approaches – the original

energetic model and the heuristic one – have been tested and their results presented separately.

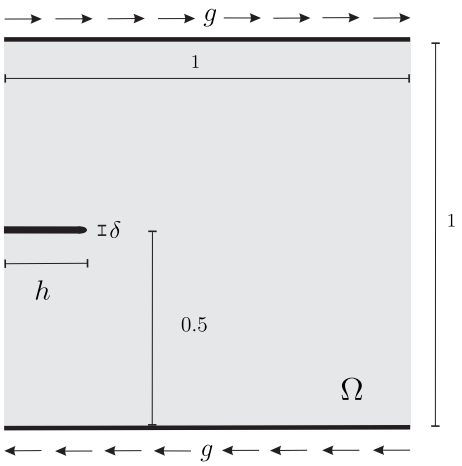

FIGURE 7. Mode II. Geometry and boundary conditions.

TABLE 2. Mode II. Parameters.

Parameter	Value	Parameter	Value
h	0,25 m	E	30 GPa
δ	0,01 m	ρ_0	10^{-6}
l	$2\delta/3$ m	ν	0,20
g	0,01 m	κ_s	4.5 $\times 10^5$ J/m

It is interesting to note that one of the characteristics of this problem lies in the symmetry of the strain energy density. Being the Francfort-Marigo model based solely on the energy density values, it is evident that damage shows two symmetric branches, one (spurious) in compression and one in traction. Figure 8 shows the topological derivative at the crack tip in the exact moment before the damage propagation.

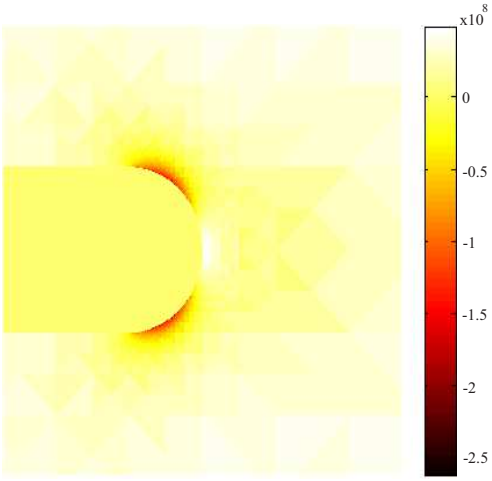

FIGURE 8. Modo II. Topological derivative.

It can be seen that there are two distinct regions ahead of the damage where the topological derivative is negative, what confirms the expectations. The final distribution

of damage can be seen in Figure 9(a), where the red spurious branch was created in a compression state, and the black one in a state of traction. This result agrees with the available results in the literature [1, 10] regarding the damage model of Francfort and Marigo. On the other hand, in Figure 9(b), the propagation is allowed to occur only when the trace of the stress tensor is positive. In this case, the damage propagation is physically consistent.

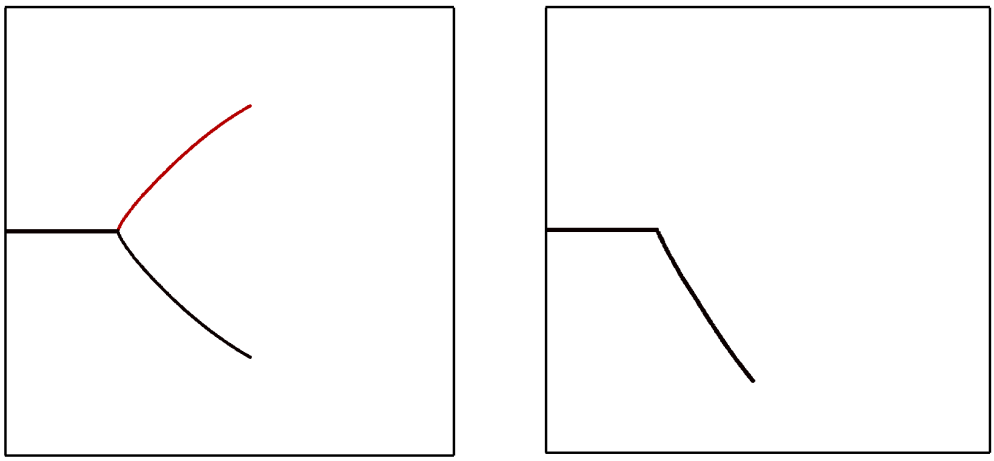

(a) original model (b) modified model

FIGURE 9. Modo II. Final results.

5.4. **Fiber Reinforced Matrix.** This case presented in [10] consists of a rigid fiber embedded in a deformable matrix. In particular, we consider a carbon's fiber embedded in a region composed by epoxy. It is assumed that the structure is under plane strain assumption and two different situations are considered. In the first one, the matrix is pulled in the upper face, then the deformable matrix is under traction state. In the second one, the matrix is pushed in the upper face inducing compression state in the matrix. The others boundaries are free. In both cases the midpoint of the fiber remains clamped to avoid translations and rotations, see Figure 10. All parameters are summarized in Table 3 where E_0 is the Young's modulus of the epoxy and E_1 the Young's modulus of the carbon's fiber. In order to avoid unrealstic damage propagation under compression state, the damage is nucleated if the condition $\mathrm{tr}(\sigma(u_i(x))) > 0$ is fulfilled, provided that the topological derivative is negative. We stress however that it can be seen as a purely heuristic strategy with no theoretical foundation.

TABLE 3. Fiber reinforced matrix. Parameters.

Parameter	Value	Parameter	Value
E_0	3,0 GPa	E_1	230,0 GPa
δ	0,0 m	ρ_0	10^{-6}
l	0,02 m	ν	0,30
g	0,1 m	κ_s	1,0 $\times 10^6$ J/m

Figures 11(a) and 11(b) shows the damage evolution for the traction and compression tests, respectively. In these examples, the propagation is allowed to occur only when the trace of the stress tensor is positive. In this case, the damage propagation is physically consistent. Note that, in both tests, the phenomenon of debonding between the fiber and

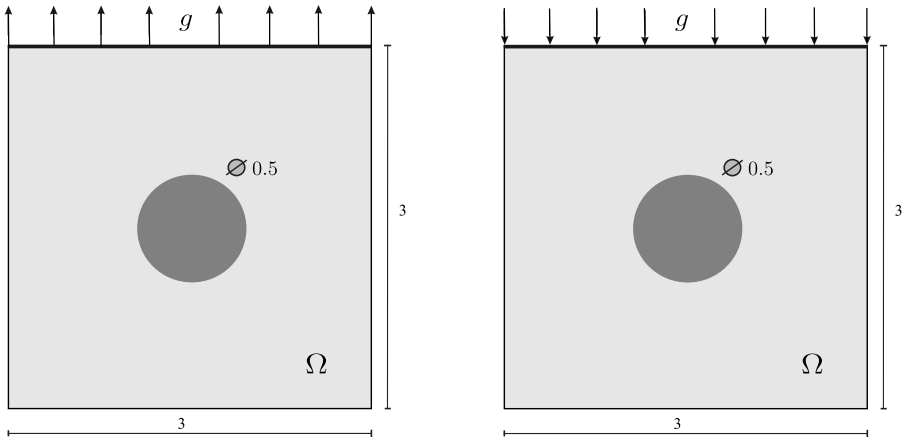

(a) traction test (b) compression test

FIGURE 10. Fiber reinforced matrix. Geometry and boundary conditions.

the matrix is captured. It is important to note that no region was previously damaged, and hence Algorithm 1 is able to nucleate and propagate damage zones simultaneously. Note that it is not clear to us if in the literature [11, 10] the damage was allowed to nucleate in the interface between the fiber and the matrix. Thus, the results obtained by other methods are not equal to those obtained by our approach, since in [11, 10] the damage was initiated and spread toward the sides. However, similar results from our approach can be observed in [1] and in the most recent reference [4] considering compression. We claim however that the result present in Figure 11(b) is just speculative, since the specimen is under compression and no eventual contact condition on the created crack lips is considered. Instead, the black branch representing the cracked zone in Figure 11(b) is filled by a damaged material, with very low Young modulus. Nevertheless, the obtained result taking into account these simplifications is promising and motivates further improvement on our model.

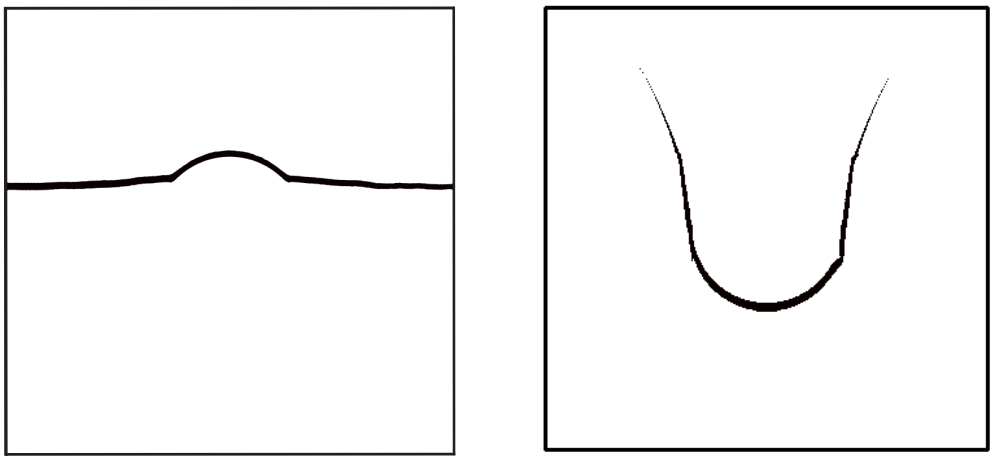

(a) traction test (b) compression test

FIGURE 11. Fiber reinforced matrix. Final results.

5.5. **Experimental Results.** Some available experimental results used to test Algorithm 1 can be found in [14]. The geometry of interest for these experiments, sometimes called Bittencourt's experiments [8], is shown in Figure 12 where all dimensions are given in

inches. In particular, we highlight the three holes located between the load and initial crack. Thus, the scope is now the study of the influence of these holes on the crack trajectory.

The different cases treated by this geometry differ by the position of the crack with respect to the applied load, given on the one hand by the distance c, and on the other hand by the dimension of the initial crack length denoted as h, which are shown in Table 4. The additional parameters used to test the algorithm are shown in Table 5.

TABLE 4. Bittencourt's experiments. Position and length of the initial damage.

	c (in)	h (in)
Bittencourt 1	5,0	1,5
Bittencourt 2	6,0	1,0

TABLE 5. Bittencourt's experiments. Parameters.

Parameters	Value	Parameters	Value
N	100	E	4,5 $\times 10^5$ psi
δ	0,005 in	ρ_0	10^{-6}
l	$2\delta/3$ in	ν	0,35
g	0,20 in	κ_s	15 (in-lbf)/in

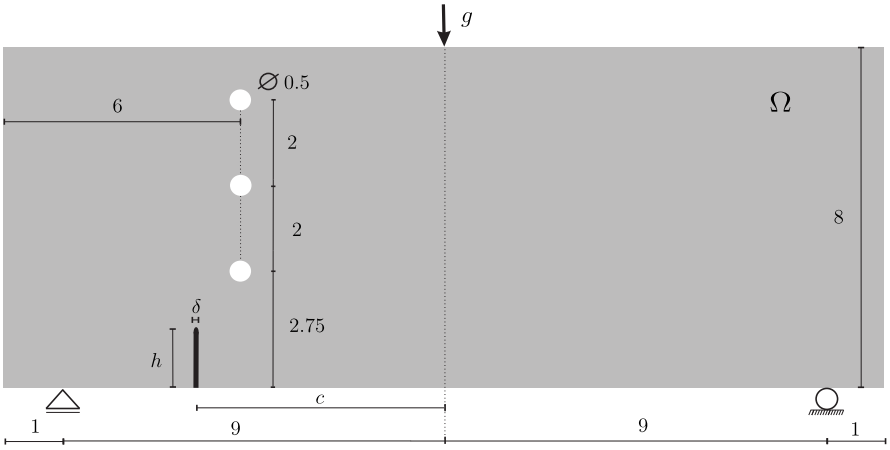

FIGURE 12. Bittencourt's experiment. Geometry and boundary conditions.

In the first case ($h = 1,5$ in and $c = 5,0$ in) the experimental trajectory does not reach the first hole, but it is immediately oriented toward the second one. The proposed algorithm was able to reproduce (almost exactly) this experimental result, as shown in Figure 13(a). In the second case ($h = 1,0$ in and $c = 6,0$ in) the experimental trajectory is oriented directly toward the second hole. Again, the proposed algorithm was able to reproduce the experimental results, as presented in Figure 13(b). Here, there the results were obtained without any heuristic approach, since the crack tip is always under traction during the whole damage processing. Similar results have been obtained in [7, 9].

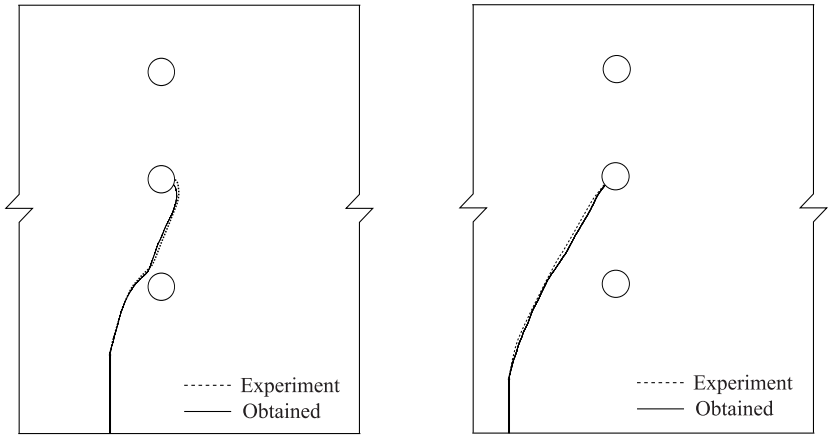

(a) case 1 (b) case 2

FIGURE 13. Bittencourt's experiment. Final results.

5.6. **Heterogeneous Medium.** In this last example we consider a heterogenous medium. The idea is to corrupt the Young modulus E with White Gaussian Noise (WGN) of zero mean and standard deviation η. Therefore, E is replaced by $E_\eta = E(1 + s\eta)$, where $s : \Omega \to \mathbb{R}$ is a function assuming random values in the interval $(0, 1)$ and $\eta = 2$ corresponds to the noise level. The domain consists of a rectangle $\Omega = (0, 1.5) \times (0, 1)$ with unit thickness (units are in m) with an initial damage of length h and width δ located at the center of the bottom side of the domain, as presented in Figure 14. The parameters used in this example are summarized in Table 6.

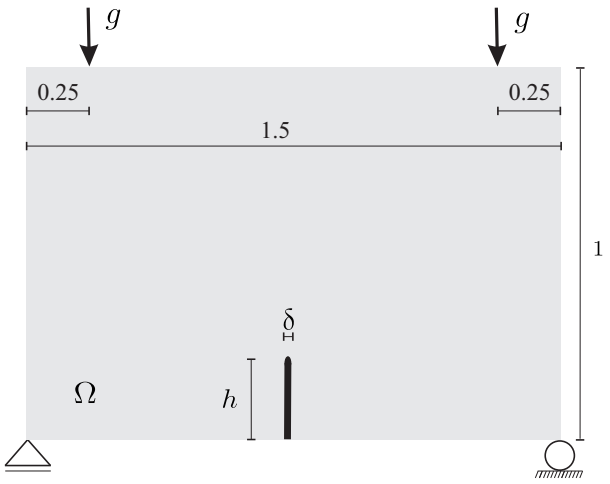

FIGURE 14. Heterogeneous case. Geometry and boundary conditions.

TABLE 6. Heterogeneous case. Parameters.

Parameter	Value	Parameter	Value
h	0,2 m	E	30 GPa
δ	0,01 m	ρ_0	10^{-6}
l	$2\delta/3$ m	ν	0,20
g	0,01 m	κ_s	5.0×10^3 J/m

The corrupted Young modulus $E_\eta(x)$ and the final result can be seen in Figures 15(a) and 15(b), respectively. It is interesting to note that due to the medium heterogeneity, we can observe kinking and bifurcations phenomena, which is in agreement with what it is spected from the physical point of view.

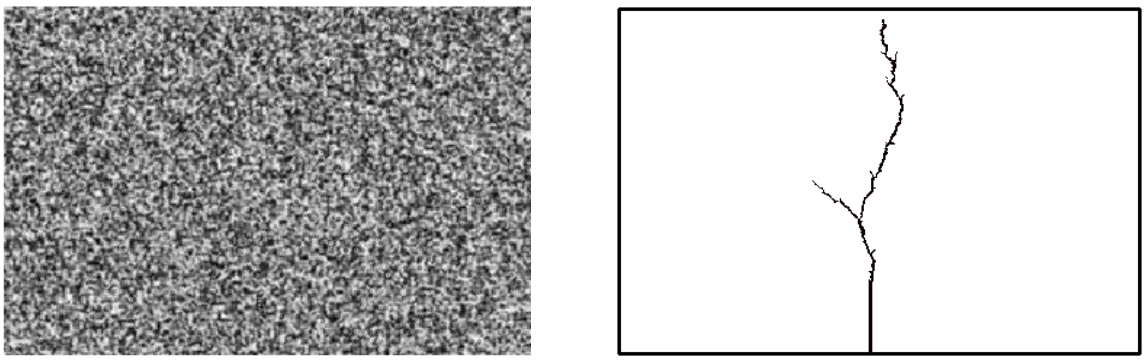

(a) corrupted Young modulus (b) final result

FIGURE 15. Heterogeneous case.

6. Concluding Remarks

In this study, we proposed an algorithm for the Francfort-Marigo damage model based solely on the topological derivative concept, which naturally allows for both nucleation and propagation of damage zones. The devised algorithm incorporates a sequence of finite perturbations according to the contour lines of the topological derivative field, which can be seen as a direct extension of the concept of infinitesimal perturbation for numerical purposes. It is important to emphasize that the topological derivative is obtained by post processing and has no significant computational cost. Indeed, as far as computational cost is concerned, the process of mesh intensification at the crack tip becomes the main bottleneck of our algorithm.

Several benchmark numerical experiments found in the current literature have been reproduced, including real life Bittencourt's experiments. It is worth to note that the present approach was able to capture important features of fracture modelling in brittle materials such as nucleation and propagation, together with kinking and bifurcations. In addition, some numerical tests using a heuristic propagation approach were presented, which allows for the distinction between states of compression and traction. While this approach is not completely novel (*cf.* [4]) the results are promising and encourage the development of the topological derivative for functionals which specifically would consider distinct criteria in traction and in compression.

However, it is well-known that such a modelling leads to a class of non-linear elasticity systems. The extension to non-linear problems in general can be considered as the main challenge associated with the theoretical development of the topological derivative method. The difficult arises when the non-linearity comes out from the main part of the operator, which at the same time suffers a topological perturbation. It is the case of nucleation of holes in plasticity and finite deformations in solid mechanics, for instance. This will be the aim of future work. Finally, we would like to highlight the striking simplicity of the proposed topological derivative-based fracture modelling summarized in Algorithm 1.

Acknowledgements

This research was partly supported by CNPq (Brazilian Research Council), CAPES (Brazilian Higher Education Staff Training Agency), ANP (National Agency of Petroleum, Natural Gas and Biofuels) and FAPERJ (Research Foundation of the State of Rio de Janeiro). These supports are gratefully acknowledged. N. Van Goethem was supported by the FCT Starting Grant "Mathematical theory of dislocations: geometry, analysis, and modelling" (IF/00734/2013).

References

[1] G. Allaire, F. Jouve, and N. Van Goethem. Damage and fracture evolution in brittle materials by shape optimization methods. *Journal of Computational Physics*, 230(12):5010–5044, 2011.

[2] L. Ambrosio and V. Tortorelli. On the approximation of free discontinuity problems. *Bollettino dell'Unione Matematica Italiana*, 6:105–123, 1992.

[3] H. Ammari and H. Kang. *Polarization and moment tensors with applications to inverse problems and effective medium theory*. Applied Mathematical Sciences vol. 162. Springer-Verlag, New York, 2007.

[4] H. Amor, J. J. Marigo, and C. Maurini. Regularized formulation of the variational brittle fracture with unilateral contact: Numerical experiments. *Journal of the Mechanics and Physics of Solids*, 57:1209–1229, 2009.

[5] S. Amstutz. Sensitivity analysis with respect to a local perturbation of the material property. *Asymptotic Analysis*, 49(1-2):87–108, 2006.

[6] S. Amstutz, C. Dapogny, and A. Ferrer. A consistent relaxation of optimal design problems for coupling shape and topological derivatives. Technical Report hal-01407486, France, 2016.

[7] P. Areias, D. Dias da Costa, J. Alfaiate, and E. Julio. Arbitrary bi-dimensional finite strain cohesive crack propagation. *Computational Mechanics*, 45:61–75, 2009.

[8] T. N. Bittencourt, P. A. Wawrzynek, A. R. Ingraffea, and J. L. Sousa. Quasi-automatic simulation of crack propagation for 2d LEFM problems. *Engineering Fracture Mechanics*, 55(2):321–334, 1996.

[9] S. Bordas and B. Moran. Enriched finite elements and level sets for damage tolerance assessment of complex structures. *Engineering Fracture Mechanics*, 73:1176–1201, 2006.

[10] B. Bourdin, G. A. Francfort, and J. J. Marigo. Numerical experiments in revisited brittle fracture. *Journal of the Mechancis and Physics of Solids*, 48:797–826, 2000.

[11] B. Bourdin, G. A. Francfort, and J. J. Marigo. The variational approach to fracture. *Journal of Elasticity*, 91(1-3):5–148, 2008.

[12] G. A. Francfort and J. J. Marigo. Stable damage evolution in a brittle continuous medium. *European Journal of Mechanics, A/Solids*, 12(2):149–189, 1993.

[13] S. M. Giusti, A. Ferrer, and J. Oliver. Topological sensitivity analysis in heterogeneous anisotropic elasticity problem. theoretical and computational aspects. *Computer Methods in Applied Mechanics and Engineering*, 311:134–150, 2016.

[14] A. R. Ingraffea and M. Grigoriu. Probabilistic fracture mechanics: A validation of predictive capability. Technical report, Cornell University, Ithaca, New York, 1990.

[15] A. Karma, D. A. Kessler, and H. Levine. Phase-field model of mode III dynamic fracture. *Physical Review Letters*, 87(045501), 2001.

[16] C. Kodsi. Crack initiation: A non-local energy approach. *Engineering Fracture Mechanics*, 165:153–182, 2016.

[17] G. Dal Maso and F. Iurlano. Fracture models as gamma-limits of damage models. *Communications on Pure and Applied Mathematics*, 12(4):1657–1686, 2013.

[18] A. A. Novotny and J. Sokołowski. *Topological derivatives in shape optimization*. Interaction of Mechanics and Mathematics. Springer-Verlag, Berlin, Heidelberg, 2013.

[19] N. Van Goethem and A. A. Novotny. Crack nucleation sensitivity analysis. *Mathematical Methods in the Applied Sciences*, 33(16):1978–1994, 2010.

(M. Xavier) Laboratório Nacional de Computação Científica LNCC/MCT, Coordenação de Matemática Aplicada e Computacional, Av. Getúlio Vargas 333, 25651-075 Petrópolis - RJ, Brasil

(E.A. Fancello) Universidade Federal de Santa Catarina EMC/UFSC, Departamento de Engenharia Mecânica, Campus Universitário, 88040-900 Florianópolis - SC, Brasil

(J.M.C. Farias) Universidade Federal de Santa Catarina EMC/UFSC, Departamento de Engenharia Mecânica, Campus Universitário, 88040-900 Florianópolis - SC, Brasil

(N. Van Goethem) Universidade de Lisboa, Faculdade de Ciências, Departamento de Matemática, CMAF+CIO, Alameda da Universidade, C6, 1749-016 Lisboa, Portugal

(A.A. Novotny) Laboratório Nacional de Computação Científica LNCC/MCT, Coordenação de Matemática Aplicada e Computacional, Av. Getúlio Vargas 333, 25651-075 Petrópolis - RJ, Brasil

E-mail address: novotny@lncc.br